

Spatial Causal Tensor Completion for Multiple Exposures and Outcomes: An Application to the Health Effects of PFAS Pollution

Xiaodan Zhou

Department of Statistics, North Carolina State University

Brian J Reich

Department of Statistics, North Carolina State University

Shu Yang*

Department of Statistics, North Carolina State University

March 18, 2026

Abstract

Per- and polyfluoroalkyl substances (PFAS) are typically encountered as mixtures of distinct chemicals with distinct effects on multiple health outcomes. Estimating joint causal effects using spatially-dependent observed data is challenging. We propose a spatial causal tensor completion framework that jointly models multiple exposures and outcomes within a low-rank tensor structure, while adjusting for observed confounders and latent spatial confounders. This method combines a low-rank tensor representation to pool information across exposures and outcomes with a spectral adjustment step that incorporates graph-Laplacian eigenvectors to approximate unmeasured spatial confounders, implemented via a projected-gradient descent algorithm. This framework enables causal inference in the presence of unmeasured spatial confounding and pervasive missingness of potential outcomes. We establish theoretical guarantees for the estimator and evaluate its finite-sample performance through extensive simulations. In an application to national PFAS monitoring data, our approach yields more conservative and credible causal relationships between PFOA and PFOS exposure and 13 chronic disease outcomes compared with existing alternatives.

Keywords: Unmeasured Spatial Confounding; Mixture Modeling; Potential Outcomes; Propensity Score; Inverse Probability Weighting.

*The authors thank Dr. Ana Rappold of the United States Environmental Protection Agency for her help accessing and interpreting the data. This work was partially supported by National Institutes of Health grants R01ES031651 and R01ES036270.

1 Introduction

Per- and polyfluoroalkyl substances (PFAS) are a class of synthetic chemicals widely used since the 1950s due to their resistance to water, oil, and heat ([Gaines 2023](#)). Because of their persistence in the environment, they are often referred to as ‘forever chemicals,’ raising substantial public health concerns. PFAS chemicals rarely occur in isolation; drinking water contamination typically involves mixtures of compounds such as PFOA and PFOS. Multiple PFAS chemicals have been associated with a range of adverse outcomes, including altered immune and thyroid function, liver disease, lipid and insulin dysregulation, kidney disease, adverse reproductive and developmental outcomes, and cancer ([Fenton et al. 2021](#)). Yet despite growing attention, evidence for many health outcomes remains inconsistent and inconclusive ([NASEM et al. 2022](#)), potentially due to the complexity of the problem.

In this work, we study the effects of PFAS exposures on multiple health outcomes. This naturally gives rise to a multiple-exposure, multiple-outcome setting. The analysis is complicated by two major challenges: first, PFAS are typically encountered as mixtures of distinct chemicals with different sources and health effects, making it difficult to isolate the contributions of individual components; second, both exposures and outcomes exhibit spatial patterns, introducing the possibility of unmeasured spatial confounding ([Reich et al. 2021](#)). These complexities motivate the development of new statistical approaches tailored to this problem.

A large statistical literature has developed to quantify the effects of exposure mixtures ([Joubert et al. 2022](#), [Kang et al. 2023](#)). Widely used approaches include weighted quantile sum regression ([Carrico et al. 2015](#)), Bayesian kernel machine regression ([Bobb et al. 2015](#)), and quantile-based g-computation ([Keil et al. 2020](#)). However, they generally focus on a single outcome and do not account for unmeasured spatial confounding. Univariate-outcome spatial methods have been proposed to adjust for spatially structured confounders ([Thaden](#)

& Kneib 2018, Papadogeorgou et al. 2019, Osama et al. 2019, Keller & Szpiro 2020, Schnell & Papadogeorgou 2020, Marques et al. 2022, Dupont et al. 2022, Guan et al. 2023, Gilbert et al. 2021, Wiecha et al. 2025) but these approaches are limited to one exposure and one outcome at a time, making them unsuitable for analyzing PFAS mixtures with multiple health endpoints.

Parallel to these developments, existing work has reframed causal effect estimation as a matrix or tensor completion problem, where counterfactual outcomes are recovered under low-rank structures (Poulos et al. 2021, Auerbach et al. 2022, Zhen & Wang 2024, Mao et al. 2024). This line of research enables principled imputation of missing potential outcomes and extends naturally to multivariate settings. However, these methods typically treat each exposure independently, overlooking latent relationships among exposures. More recent approaches integrate exposures into a single tensor representation, allowing for joint modeling of exposure effects and improved efficiency, as demonstrated in Abadie et al. (2024), Agarwal et al. (2020), Gao et al. (2024), and Gao et al. (2025).

Two recent parallel works also address multiple exposures and outcomes with spatial confounding, though with different strategies. Prim et al. (2025) propose a spectral confounder adjustment that uses a three-way tensor over exposure, outcome, and spatial scale to model causal effect, assuming that confounding bias dissipates at more local spatial scales. Our approach is more general in that we use a tensor for the potential outcomes, rather than using tensors as components of a linear model. Wu & Franks (2025) develop a latent factor panel approach for spatiotemporal data that leverages repeated temporal observations to identify causal effects under a factor confounding assumption, where unmeasured confounders are captured by low-dimensional latent factors that evolve over time, combined with partial interference assumptions that limit the degree of spatial spillover. By contrast, we propose a spatial causal tensor completion framework specifically designed

for cross-sectional spatial data with multiple binary exposures and multiple outcomes.

Our method combines a low-rank Tucker tensor representation (Kolda & Bader 2009) to pool information across exposures and outcomes with a spectral adjustment step that incorporates graph-Laplacian eigenvectors to approximate unmeasured spatial confounders, implemented via a spatial projected-gradient descent algorithm. Unlike panel approaches that exploit temporal variation, our framework relies on spatial smoothness assumptions to enable causal inference in the presence of spatially patterned unmeasured confounding and pervasive missingness of potential outcomes. We establish rigorous theoretical guarantees, including Frobenius error bounds for the estimated potential outcomes tensor that decompose into interpretable components, and provide uncertainty quantification of average treatment effects through doubly robust variance estimation. We demonstrate the framework’s advantages through extensive simulations and an application to an national PFAS monitoring data. Our analysis covers 5,495 public water systems across 47 states and 13 chronic disease outcomes, reflecting typical contemporary drinking-water exposure levels rather than extreme contamination scenarios. We find that most previously reported PFAS–health associations are substantially attenuated after adjustment for spatial confounding. However, PFOS exposure remains significantly associated with elevated risk of hypertension, tooth loss, asthma, and obesity—associations that persist after adjustment and thus appear less likely to reflect geographic artifacts alone. These findings underscore the importance of accounting for spatial confounding in environmental health studies and suggest that targeted concerns about PFOS warrant continued attention.

This work makes three primary contributions. First, we develop a unified causal inference framework that jointly models multiple exposures and outcomes through low-rank tensor completion, enabling efficient estimation of factorial treatment effects in environmental mixtures studies. Second, we integrate graph-Laplacian spectral adjustment into the tensor

completion procedure to account for unmeasured spatial confounding—a pervasive challenge in environmental epidemiology. Third, we establish theoretical guarantees for the proposed estimator and validate its finite-sample performance through simulations. Our application to national PFAS data provides a large-scale, spatially-adjusted assessment of drinking-water PFOA and PFOS exposure on chronic disease outcomes, yielding more conservative and credible effect estimates than existing methods.

The remainder of the paper is organized as follows. Section 2 describes the motivating dataset. Sections 3 and 4 present the proposed methodology and its theoretical properties, with additional empirical evaluations reported in **Supplement D**. Section 5 applies the proposed approach to the motivating data. Section 6 concludes.

2 PFAS Data Description

The EPA’s PFAS Analytics Tools ([US EPA 2024](#)) provide national-level PFAS data in Public Water Systems (PWS). UCMR5 reports multiple PFAS chemicals. Among these, PFOA and PFOS are the most frequently detected compounds, while the remaining chemicals were detected at only a small number of locations. Therefore, we focus on PFOA and PFOS in this study.

The EPA establishes minimum reportable limits (MRL) as the lowest measurable concentration of a contaminant that is achievable by the majority of participating laboratories, independently of the contaminant health effects. For this reason, most often only the presence or absence of the chemical above the MRL is used as the exposure measure. In addition, the health-based Maximum Contaminant Level Goals (MCLGs) defined by EPA for PFOA and PFOS are both zero ppt (also expressed as ng/L). Therefore, the exposure is taken to be the binary indicator of detectable PFOA and/or PFOS, given four possible exposure levels: Neither PFOA or PFAS, only PFOA exposure, only PFOS exposure, and

both PFOA and PFOS exposures.

We use health outcome data provided by the Centers for Disease Control and Prevention (CDC) PLACES dataset (CDC 2023), which contains model-based census tract-level estimates of disease prevalence among the adult population. The 13 health outcomes are: arthritis (ARTHRITIS), hypertension (BPHIGH), cancer (non-skin) or melanoma (CANCER), asthma (CASTHMA), coronary heart disease (CHD), chronic obstructive pulmonary disease (COPD), diagnosed diabetes (DIABETES), high cholesterol among adults who have ever been screened (HIGHCHOL), chronic kidney disease (KIDNEY), depression (MHLTH), obesity (OBESITY), stroke (STROKE), and all tooth loss among adults aged ≥ 65 years (TEETH). Demographic covariates were obtained from the 2020 US Census Bureau via the `tidycensus` R package (Walker et al. 2021); specific covariates are described in Section 5.

Health outcomes and demographic covariates were linked to PWS using area-weighted averaging to aggregate tract-level variables to the PWS level (Supplement C.1). This yielded 5,495 PWS samples across 47 states in the continental United States. The Table in Supplement C.2 summarizes PWS-level exposure groups and outcomes.

3 Spatial Causal Tensor Model

In this section, we introduce our spatial causal tensor framework and estimation strategy. Section 3.1 introduces notations, Section 3.2 formalizes the potential-outcomes setup, and Section 3.3 states the required causal assumptions. Section 3.4 then outlines a three-step estimator with a spatial projected gradient descent (S-PGD) algorithm.

3.1 Notations and Tensor Operations

Lowercase letters (e.g., x, y) denote scalars; bold lowercase letters (e.g., \mathbf{x}, \mathbf{y}) denote vectors; bold uppercase letters (e.g., \mathbf{A}, \mathbf{B}) denote matrices; calligraphic uppercase letters (e.g., $\mathcal{X}, \mathcal{Y}, \mathcal{Z}$) denote tensors. A tensor $\mathcal{X} \in \mathbb{R}^{N_1 \times N_2 \times N_3}$ is a 3-way array indexed by (i_1, i_2, i_3) , where $i_k \in [N_k]$, and $[N_k] = \{1, \dots, N_k\}$. The Frobenius norm of \mathcal{X} is defined as $\|\mathcal{X}\|_F^2 = \sum_{i_1, i_2, i_3} \mathcal{X}_{i_1 i_2 i_3}^2$. The spectral and nuclear norms of tensors are defined formally in **Supplement A**. The inner product is $\langle \mathcal{X}, \mathcal{Y} \rangle = \sum_{i,l,o} \mathcal{X}_{ilo} \mathcal{Y}_{ilo}$. The mode- k unfolding of a tensor $\mathcal{X} \in \mathbb{R}^{N_1 \times \dots \times N_d}$ rearranges the tensor into a matrix by aligning the mode- k fibers, a one-dimensional slice of a tensor obtained by fixing all indices but one, as columns of the resulting matrix, $\mathcal{X}_{(1)} \in \mathbb{R}^{N_1 \times (N_2 N_3)}$, $\mathcal{X}_{(2)} \in \mathbb{R}^{N_2 \times (N_1 N_3)}$, $\mathcal{X}_{(3)} \in \mathbb{R}^{N_3 \times (N_1 N_2)}$. The mode- k tensor-matrix product, denoted $\mathcal{X} \times_k \mathbf{M}$, with $\mathbf{M} \in \mathbb{R}^{r \times N_k}$, yields a tensor of dimension where mode k is replaced by r . For example, $\mathcal{X} \times_1 \mathbf{M} \in \mathbb{R}^{r \times N_2 \times N_3}$. This operation involves unfolding \mathcal{X} along mode k , applying matrix multiplication, and refolding to the tensor form. For a comprehensive introduction to tensor operations, see [Kolda & Bader \(2009\)](#).

3.2 Tensor Formulation of Potential Outcomes

Our proposed method is a novel attempt to impute the missing potential outcomes using low-rank tensor completion under the potential outcomes framework. Suppose there are N observational units, each exposed to a K -dimensional binary exposure vector $\mathbf{A}_i \in \{0, 1\}^K$, which defines $L = 2^K$ possible exposure combinations. We index each exposure combination by its decimal equivalent, denoted $\ell_i \in \{1, \dots, L\}$. For clarity, let $\mathbf{a}^{(\ell)} \in \{0, 1\}^K$ represent the binary exposure vector corresponding to exposure level ℓ . For example, when $K = 2$, if $\mathbf{A}_i = (A_{i1}, A_{i2})$, then $\ell_i = A_{i1} + 2A_{i2}$. In the motivating example, $N = 5,495$ denotes the number of geographic units (PWS) and $K = 2$ represents two PFAS exposure variables (PFOA and PFOS).

Under the potential outcomes framework (Rubin 1974), each unit i has a set of potential outcomes $\{\mathcal{Y}_{i\ell o} : \ell = 1, \dots, L, o = 1, \dots, O\}$, one for every possible exposure combination ℓ and outcome dimension o . In the PFAS analysis, $O = 13$ outcomes are considered, as listed in Section 2. Only the outcome corresponding to the realized exposure is observed, while the others remain counterfactual. We organize these outcomes into a tensor $\mathcal{Y} \in \mathbb{R}^{N \times L \times O}$ (left of Figure 1). Similarly, the treatment assignment is represented by the tensor $\mathcal{A} \in \mathbb{R}^{N \times L \times O}$, with $\mathcal{A}_{i\ell o} = 1$ if unit i received exposure ℓ , and $\mathcal{A}_{i\ell o} = 0$ otherwise. Note that $\mathcal{A}_{i\ell o}$ does not vary across the third outcome-mode dimension, so it effectively reduces to an $N \times L$ matrix. We maintain the tensor representation for consistency with the outcome tensor and to simplify presentation. Each unit receives one exposure, i.e. $\sum_{\ell} \mathcal{A}_{i\ell o} = 1$.

We assume that the observed outcome tensor follows a low-rank Tucker decomposition (Right of Figure 1):

$$\mathcal{Y} = \mathcal{Y}^* + \mathcal{E} = \mathcal{G} \times_1 \mathbf{U}_1 \times_2 \mathbf{U}_2 \times_3 \mathbf{U}_3 + \mathcal{E}, \quad \mathcal{E} \stackrel{iid}{\sim} \text{sub-Gaussian}(0, \sigma^2). \quad (1)$$

In (1), $\mathcal{G} \in \mathbb{R}^{r_1 \times r_2 \times r_3}$ is the core tensor and $\mathbf{U}_1 \in \mathbb{R}^{N \times r_1}$, $\mathbf{U}_2 \in \mathbb{R}^{L \times r_2}$ and $\mathbf{U}_3 \in \mathbb{R}^{O \times r_3}$ are factor matrices corresponding to spatial, exposure, and outcome variation, respectively. To capture both measured and unmeasured sources of spatial variation, we model $\mathbf{U}_1 = \mathbf{Z}\boldsymbol{\eta}_Z + \mathbf{S}\boldsymbol{\eta}_S$, where $\mathbf{Z} \in \mathbb{R}^{N \times r_1}$ are measured covariates with effect $\boldsymbol{\eta}_Z \in \mathbb{R}^{r_1 \times r_1}$, and $\mathbf{S} \in \mathbb{R}^{N \times r_1}$ are unmeasured spatial components with effect $\boldsymbol{\eta}_S \in \mathbb{R}^{r_1 \times r_1}$. By unmeasured spatial confounder, we refer to latent variables that exhibit spatial structure and simultaneously influence exposures and outcomes. The measured covariates \mathbf{Z} and unmeasured spatial confounding \mathbf{S} jointly affect both the outcomes and the treatment assignment mechanism, as described below.

In this representation, r_1 , r_2 and r_3 are less than or equal to N , L , and O , respectively. The factor matrices \mathbf{U} can be viewed as the principal components in each mode, and the entries

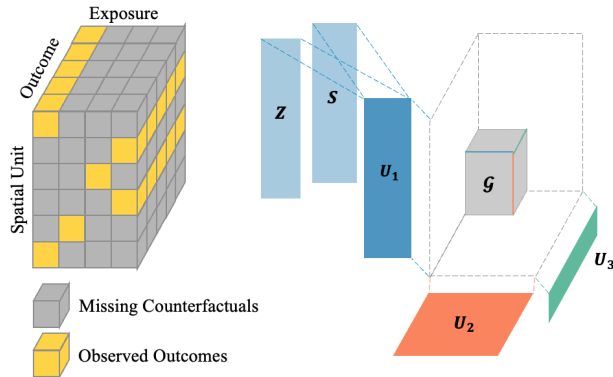


Figure 1: Illustration of the spatial causal tensor decomposition. Left: a tensor of counterfactual outcomes, where observed entries (yellow) and missing entries (gray) are arranged by spatial units (PWS), exposures, and outcomes. Right: Tucker decomposition into spatial (\mathbf{U}_1), exposure (\mathbf{U}_2), and outcome (\mathbf{U}_3) factors with a low-rank core \mathcal{G} . The spatial factor \mathbf{U}_1 is further expressed as a combination of measured covariates \mathbf{Z} and latent spatial components \mathbf{S} . The illustration omits the noise term \mathcal{E} for clarity.

in \mathcal{G} entail the level of interaction between different components. The low-rank assumption on \mathcal{Y}^* can be justified in the following way. First, the heterogeneity among locations may be attributed to r_1 latent spatial factors; e.g., sociodemographic trends. Second, the variation from the PFAS exposure may be summarized into r_2 key factors, such as chemicals with shared sources or physical, cheminformatic properties. Finally, the multiple health responses may be related due to r_3 hidden biological pathways.

Our parameter of interest is the average treatment effect (ATE) defined for any exposure ℓ (relative to the reference level L) and outcome o by: $\theta_{\ell o}^* = \mathbb{E}\left(\sum_{i=1}^N (\mathcal{Y}_{i\ell o} - \mathcal{Y}_{iLo}) / N\right)$.

3.3 Causal Assumptions

To formalize the exposure mechanism, the exposure probability for unit i (with covariates \mathbf{Z}_i and unobserved spatial factor \mathbf{S}_i) to receive exposure ℓ is

$$\pi(\ell \mid \mathbf{Z}_i, \mathbf{S}_i) = \mathbb{P}(\mathbf{A}_i = \mathbf{a}^{(\ell)} \mid \mathbf{Z}_i, \mathbf{S}_i). \quad (2)$$

We adopt the following classical causal assumptions to justify our estimating strategy.

Assumption 1 (SUTVA; Stable Unit Treatment Value Assumption) (1) *the po-*

tential outcomes for any unit do not vary with the treatment assigned to other units;
(2) there are no different versions of each treatment level leading to different potential outcomes.

Assumption 1 rules out interference between geographic units and requires that each exposure condition is well-defined. The no-interference component requires that PFAS exposure in one geographic unit does not affect health outcomes in another. This is plausible in our setting because exposure is measured through drinking water systems that serve distinct populations. Potential violations could nonetheless arise through population mobility or environmental contamination spreading between neighboring regions. We interpret our results as direct effects of local drinking water exposure, acknowledging that spillover effects, if present, are not captured. The consistency component requires careful interpretation: our binary exposure indicator aggregates heterogeneous concentration levels above the detection limit. Consequently, estimated effects represent averages over the observed distribution of exposure intensities rather than effects of a precisely defined exposure level.

Assumption 2 (Latent Ignorability) $\mathbf{A}_i \perp \{\mathcal{Y}_{i\ell o} : \ell, o\} \mid (\mathbf{Z}_i, \mathbf{S}_i)$. *In other words, \mathbf{Z}_i and \mathbf{S}_i account for all confounders influencing treatments and outcomes.*

Assumption 2 extends the standard no-unmeasured-confounding condition by allowing for unobserved spatial confounders, such as unmeasured industrial activity or correlated environmental exposures that vary smoothly over space. We model these through low-dimensional latent spatial components approximated via spectral adjustment using the graph Laplacian eigenbasis. This approach is effective for confounders varying at spatial scales captured by the selected eigenvectors, but may fail for confounders varying at finer scales than our adjacency structure can resolve or for confounders that lack spatial structure altogether. The main threats to this assumption include: non-spatial confounders not captured by our measured covariates (such as bottled water); and temporal misalignment,

as our exposure measurements (2023–2024) and health outcomes (2017–2018) span different periods, though the long environmental persistence and biological half-lives of PFAS partially mitigate this concern.

Assumption 3 (Latent Positivity) *There exists a constant $p_{\min} \in (0, \frac{1}{2})$ such that for every unit i and exposure level $\ell \in \{1, \dots, L\}$, $p_{\min} \leq \mathbb{P}(\mathbf{A}_i = \mathbf{a}^{(\ell)} \mid \mathbf{Z}_i, \mathbf{S}_i) \leq 1 - p_{\min}$. That is, each unit has a nonzero probability of receiving any exposure combination, ruling out deterministic assignment by covariates or location.*

Assumption 3 requires that each exposure combination has nonzero probability of occurring, ruling out deterministic assignment by geography or covariates. Limited overlap is a known challenge in environmental studies, particularly when contamination is highly localized. We empirically assess this assumption by examining the distribution of estimated propensity scores in our application (**Table 3 in Supplement C.2**). The results indicate moderate overlap: only limited units have propensity scores below 0.01, though a notable fraction of exposed units (10 to 48%) have scores below 0.05, with the PFOA-only and PFOS-only groups exhibiting the most limited support.

3.4 A Three-Step Estimating Procedure

We proceed in three steps. Step 1 uses an unweighted S-PGD fit with a Laplacian eigenbasis to learn the latent spatial component $\hat{\mathbf{S}}^{(0)}$ while estimating the Tucker factors from observed entries. Step 2 fits the exposure model $\hat{\pi}(\ell \mid \mathbf{Z}_i, \hat{\mathbf{S}}_i^{(0)})$ and constructs inverse-probability weights $\hat{\mathcal{W}}^{(0)}$ that account for exposure-induced missingness. Step 3 re-runs S-PGD with the weights to re-estimate the spatial component and complete the full potential-outcome tensor, yielding $\hat{\mathbf{S}}$ and $\hat{\mathcal{Y}}$, and thus the final ATE estimates.

3.4.1 Step 1: Spectral adjustment for spatial confounding

Let \mathbf{Q} be the graph Laplacian built from the spatial adjacency matrix, with eigendecomposition $\mathbf{Q} = \mathbf{\Phi} \mathbf{\Lambda} \mathbf{\Phi}^\top$. Low-frequency eigenvectors in $\mathbf{\Phi}$ capture broad spatial trends. We assume the unmeasured spatial component \mathbf{S} follows a Gaussian Markov random field that can be well-approximated by the span of the first k low-frequency eigenvectors,

$$\mathbf{S} \approx \mathbf{\Phi}_{1:k} \boldsymbol{\beta}, \quad \mathbf{U}_1 \approx \mathbf{Z} \boldsymbol{\eta}_Z + \mathbf{\Phi}_{1:k} \boldsymbol{\beta},$$

we denote $[\mathbf{\Phi}_1, \mathbf{\Phi}_2, \dots, \mathbf{\Phi}_k]$ as $\mathbf{\Phi}_{1:k}$, with $\boldsymbol{\beta} \in \mathbb{R}^{k \times r_1}$ are the corresponding coefficients. We obtain $\widehat{\mathbf{S}}^{(0)}$ by minimizing the unweighted reconstruction loss

$$\arg \min_{\mathcal{G}, \mathbf{U}_2, \mathbf{U}_3, \boldsymbol{\eta}_Z, \boldsymbol{\beta}} \left\{ \|\mathcal{A} \circ (\mathcal{Y} - \mathcal{G} \times_1 (\mathbf{Z} \boldsymbol{\eta}_Z + \mathbf{\Phi}_{1:k} \boldsymbol{\beta}) \times_2 \mathbf{U}_2 \times_3 \mathbf{U}_3)\|_F^2 \right\}.$$

using the S-PGD solver described in Section 3.4.4. This step provides an initial estimate of the latent spatial component.

3.4.2 Step 2: Propensity score and weight estimation

By Assumptions (1)–(3), inverse-probability weighting creates a pseudo-population in which exposure assignment is independent of the potential outcomes. Consequently, the exposure-induced missingness in \mathcal{Y} is ignorable after weighting, enabling unbiased tensor completion under the Tucker model. Specifically, we estimate the exposure probabilities $\widehat{\pi}(\ell | \mathbf{Z}_i, \widehat{\mathbf{S}}_i^{(0)})$ using multinomial logistic regression, and further construct inverse probability weights $\widehat{\mathcal{W}}^{(0)}$,

$$\widehat{\pi}(\ell | \mathbf{Z}_i, \widehat{\mathbf{S}}_i^{(0)}) = \mathbb{P}(\mathbf{A}_i = \mathbf{a}^{(\ell)} | \mathbf{Z}_i, \widehat{\mathbf{S}}_i^{(0)}), \quad \widehat{\mathcal{W}}_{i\ell o}^{(0)} = \frac{\mathbf{1}(\mathbf{A}_i = \mathbf{a}^{(\ell)})}{\widehat{\pi}(\ell | \mathbf{Z}_i, \widehat{\mathbf{S}}_i^{(0)})}, \quad \forall \ell,$$

where the indicator function $\mathbf{1}(\mathbf{A}_i = \mathbf{a}^{(\ell)})$ ensures that weights are only applied to observed exposure-outcome pairs. Since inverse weighting can become unstable in settings with many

treatment categories, calibration weighting may be employed as a more stable alternative (Yang 2018, Gao et al. 2023).

3.4.3 Step 3: Weighted Tensor Completion

In Step 1, the initial spatial component $\widehat{\mathbf{S}}^{(0)}$ is learned from an *unweighted* tensor fit that does not yet account for the exposure mechanism. Using the weights from Step 2, we re-estimate both the spatial component and the tensor to correct for exposure-induced selection, yielding refined $\widehat{\mathbf{S}}$ and $\widehat{\mathcal{Y}}$. Specifically, we refit the tensor with a weighted loss,

$$\arg \min_{\mathcal{G}, \mathbf{U}_2, \mathbf{U}_3, \boldsymbol{\eta}_Z, \boldsymbol{\beta}} \left\{ \left\| \sqrt{\widehat{\mathcal{W}}^{(0)}} \circ \mathcal{A} \circ (\mathcal{Y} - \mathcal{G} \times_1 (\mathbf{Z} \boldsymbol{\eta}_Z + \boldsymbol{\Phi}_{1:k} \boldsymbol{\beta}) \times_2 \mathbf{U}_2 \times_3 \mathbf{U}_3) \right\|_F^2 \right\},$$

using the S-PGD. This reweighted tensor fit provides the completed potential-outcome tensor $\widehat{\mathcal{Y}}$, which can directly feed into the average treatment effector estimators with standard errors described in Section 4.3.

3.4.4 Spatial Projected Gradient Descent Algorithm

Classical PGD implicitly assumes a fixed projection space for factors in any mode. In contrast, in the S-PGD algorithm—which we use in Steps 1 and 3 above—updates the projection space by selecting Laplacian eigenvectors in a stepwise fashion. At each step, we expand the projection by one candidate eigenvector, using warm-start from the previous solution, and retain the expansion only if it improves a BIC-type criterion. This allows the algorithm to adaptively capture spatial structure rather than committing to a pre-specified set of eigenvectors. In the above, the Tucker ranks r_1, r_2, r_3 are assumed to be known. In practice, they are selected via cross-validation in Step 1 of the estimating procedure. Complete algorithmic details, including BIC criterion, warm-start initialization scheme and stopping criteria, are provided in **Supplement B**.

4 Theoretical Properties

4.1 Tensor Structural Assumptions

Before presenting our main theorem, we introduce additional structural assumptions on the latent spatial variables and on the low-rank tensor model. These assumptions provide the technical foundation needed to establish the asymptotic bounds for our weighted spatial tensor completion estimator.

Assumption 4 (Unmeasured Smooth Spatial Variables) *Let $\mathbf{S} \in \mathbb{R}^{N \times r_1}$ denote r_1 smooth graph signals over a connected, undirected graph $G = (V, E)$ with $|V| = N$. Let \mathbf{Q} be the normalized graph Laplacian with eigendecomposition $\mathbf{Q} = \mathbf{\Phi} \mathbf{\Lambda} \mathbf{\Phi}^\top$, where $\mathbf{\Phi} = [\phi_1, \dots, \phi_N]$, where $\mathbf{\Phi}$ has orthonormal columns, and $0 = \lambda_1 \leq \lambda_2 \leq \dots \leq \lambda_N$. Assume that each column $\mathbf{S}^{(\ell)}$ of \mathbf{S} admits the spectral expansion: $\mathbf{S}^{(\ell)} = \sum_{j=1}^N c_j^{(\ell)} \phi_j$, with $|c_j^{(\ell)}| \leq C \cdot j^{-\alpha/\beta}$, for some constants $C > 0$ and $\alpha > \beta > 0$, uniformly over $\ell = 1, \dots, r_1$.*

Assumption 4 formalizes the idea that unmeasured spatial confounders vary smoothly over geography. By requiring that their eigen-expansion coefficients decay at a polynomial rate, this assumption ensures that most of the spatial variation is captured by a small number of the leading eigenvectors of the Laplacian.

Assumption 5 (Incoherent Tensor Parameter) *Assume $\mathbf{U}_1, \mathbf{U}_2$ and \mathbf{U}_3 have orthogonal columns, and there exists some constant μ_0 and μ_1 such that $\mathcal{Y}^* \in \mathcal{C}(r_1, r_2, r_3, \mu_0, \mu_1)$, where*

$$\max \left\{ \frac{N}{r_1} \|\mathbf{U}_1\|_{2,\infty}^2, \frac{L}{r_2} \|\mathbf{U}_2\|_{2,\infty}^2, \frac{O}{r_3} \|\mathbf{U}_3\|_{2,\infty}^2 \right\} \leq \mu_0, \quad \max_{k \in \{1,2,3\}} \|\mathcal{M}^{(k)}(\mathcal{G})\| \leq \mu_1 \sqrt{\frac{NLO}{\mu_0^{3/2} (r_1 r_2 r_3)^{1/2}}},$$

where for matrix \mathbf{V} , define $\|\mathbf{V}\|_{2,\infty}^2 = \max_i \|\mathbf{V}_i\|^2$ and \mathbf{V}_i is the i -th row vector of \mathbf{V} .

Assumption 5 is common in the matrix/tensor completion literature (Candes & Plan 2010,

Candes & Recht 2009). Incoherent matrices represent a class where each entry contains a comparable amount of information, making it feasible to complete the matrix from a small number of observations. In practice, this assumption states that information about outcomes is reasonably distributed across geographic units, exposures, and diseases.

4.2 Asymptotic Bounds

In this section, we establish the asymptotic consistency of the estimated parameter tensor $\hat{\mathcal{Y}}$ obtained by the proposed spatial tensor completion method. We present a simplified version of our main result here; the complete theorem statement with full technical conditions is provided in **Supplement A.2**.

Theorem 1 (Frobenius Error Bound - Simplified Version) *Under Assumptions (1)–(5), with probability at least $1 - 4(N + L + O)^{-2}$, our estimator satisfies:*

$$\frac{\|\Delta\|_F^2}{NO} \leq \max \left\{ A_1, A_2, A_3, A_4, A_5 \right\},$$

where

$$\begin{aligned} A_1 &= \frac{\mu_1^2 \log(N + L + O)}{p_{\min} N}, \\ A_2 &= C \frac{(r_1 \wedge r_2)^{1/2} r_3^{3/4}}{(r_1 r_2)^{1/4}} \frac{p_{\max}}{p_{\min}^2} \sigma \sqrt{r_1} k^{-\tau_2} \sqrt{\frac{L \log(N + L + O)}{O}}, \\ A_3 &= C' \left(\frac{(r_1 \wedge k) r_2 r_3}{\max\{r_1 \wedge k, r_2, r_3\}} + \frac{\mu_1^2 (r_1 \wedge r_2) r_3^{3/2}}{\mu_0^{3/2} (r_1 r_2)^{1/2} p_{\min}^2} \right) \frac{p_{\max}^2 \sigma^2 \log(N + L + O)}{p_{\min}^4 O}, \\ A_4 &= C'' \frac{p_{\max}}{p_{\min}^3} \sigma^2 \sqrt{r_1} k^{-\tau_1} \left(1 + C_5 \sqrt{\frac{\log(N + L + O)}{NO}} \right), \\ A_5 &= C''' \frac{(r_1 \wedge k) r_2 r_3 (r_1 \vee r_2 \vee r_3)^2}{\max\{r_1 \wedge k, r_2, r_3\}} \frac{1}{p_{\min}^2} \frac{(N \vee O) \log(N + L + O)}{NO}, \end{aligned}$$

where $a \wedge b$, $a \vee b$ denote the minimum and maximum of a and b respectively.

We provide detailed interpretations of each error component in **Supplement A.2**.

4.3 Average Treatment Effect

After tensor completion, we estimate the average treatment effect $\theta_{\ell o}^* = \mathbb{E}[N^{-1} \sum_{i=1}^N (\mathcal{Y}_{i\ell o} - \mathcal{Y}_{iLo})]$ comparing exposure ℓ to reference exposure L for outcome o . Given the imputed potential outcomes, the outcome imputation (OI) estimator is given by:

$$\hat{\theta}_{\ell o}^{(\text{OI})} = \frac{1}{N} \sum_{i=1}^N (\hat{\mathcal{Y}}_{i\ell o} - \hat{\mathcal{Y}}_{iLo}).$$

By Cauchy-Schwarz inequality and Theorem 1, this estimator satisfies $|\hat{\theta}_{\ell o}^{(\text{OI})} - \theta_{\ell o}^*| \leq \|\hat{\mathcal{Y}} - \mathcal{Y}^*\|_F / \sqrt{N}$. However, the OI estimator does not achieve \sqrt{N} -consistency because tensor completion converges at a slower rate than \sqrt{N} determined by the terms in Theorem 1. To achieve \sqrt{N} -consistency and enable valid asymptotic inference, we construct the augmented inverse probability weighting (AIPW) estimator (Bang & Robins 2005):

$$\begin{aligned} \hat{\theta}_{\ell o}^{(\text{AIPW})} = \frac{1}{N} \sum_{i=1}^N & \left[\left(\hat{\mathcal{Y}}_{i\ell o} + \frac{\mathbf{1}(\mathbf{A}_i = \ell)}{\hat{\pi}(\ell | \mathbf{Z}_i, \hat{\mathbf{S}}_i)} (Y_{io}^{(\mathbf{A}_i)} - \hat{\mathcal{Y}}_{i\ell o}) \right) \right. \\ & \left. - \left(\hat{\mathcal{Y}}_{iLo} + \frac{\mathbf{1}(\mathbf{A}_i = L)}{\hat{\pi}(L | \mathbf{Z}_i, \hat{\mathbf{S}}_i)} (Y_{io}^{(\mathbf{A}_i)} - \hat{\mathcal{Y}}_{iLo}) \right) \right]. \end{aligned}$$

The AIPW estimator enjoys rate double robustness: it achieves \sqrt{N} -consistency when the outcome model and the propensity score model are consistently estimated, with the product of their estimation errors being of smaller order than $N^{-1/2}$, which permits the use of flexible modeling approaches (Chernozhukov et al. 2018). In our setting where both models share the spatial component, double robustness applies conditionally on adequate spatial approximation $\hat{\mathbf{S}}$ and depends on which term in Theorem 1 dominates. Detailed conditions for \sqrt{N} -consistency are provided in **Supplement A.3**. Variance is estimated via the empirical influence function, and $100(1 - \alpha)\%$ confidence intervals are constructed

as $\hat{\theta}_{\ell_o}^{(\text{AIPW})} \pm z_{\alpha/2} \sqrt{\widehat{V}_{\ell_o}/N}$, where $\widehat{V}_{\ell_o} = N^{-1} \sum_{i=1}^N \widehat{\text{IF}}_i^2$ with details in **Supplement A.3**.

4.4 Simulation Summary

We conducted a simulation study to evaluate finite-sample performance; full details are provided in Supplement D. Using a 20×20 spatial grid with two binary exposures and ten outcomes, we compared our proposed spatial tensor method against alternatives including non-spatial tensor completion, regression, and kriging-based method. Across settings varying in tensor complexity, strength of spatial confounding, outcome noise, and exposure overlap, our method achieved the lowest or near-lowest mean squared error while maintaining appropriate coverage for confidence intervals. These results confirm that jointly modeling exposures and outcomes within a low-rank tensor framework, combined with spectral adjustment for spatial confounding, yields efficiency gains over outcome-by-outcome approaches.

5 PFAS Health Effect Analysis

5.1 Study Design

We apply our method to examine the effects of PFAS exposures on adult chronic disease outcomes, focusing on PFOA and PFOS. Outcomes include disease rates of 13 common chronic conditions, each preprocessed by shifting to ensure positivity, applying a logarithmic transformation, and scaling the entire tensor to have zero mean and unit variance. The same transformations are applied to all competing methods.

Our study provides broader population coverage than most prior PFAS health investigations, encompassing 5,495 public water systems serving approximately 24.8 million people across 47 states. Importantly, the exposure levels we analyze are relatively low (mean concentrations

of 0.00373 ng/L for PFOA and 0.00498 ng/L for PFOS among exposed systems), reflecting typical contemporary U.S. drinking-water conditions rather than highly contaminated sites. This contrasts with earlier studies focused on heavily polluted regions with substantially higher exposures. For example, [Biggeri et al. \(2024\)](#) examined a population exposed to markedly elevated drinking-water PFAS concentrations in the Veneto region of Italy, while [Barry et al. \(2013\)](#) investigated the Mid-Ohio Valley cohort using directly measured serum PFAS concentrations, which provide more precise exposure quantification than environmental water measurements. Our contribution lies in conducting a large-scale assessment of low-level, population-representative drinking-water exposure. However, this approach necessarily relies on environmental monitoring data rather than individual biomarker measurements, which limits our ability to capture variation in individual absorption, metabolism, and cumulative exposure from non-water sources.

Figure 2 depicts the conceptual structure of the study. Our primary focus is PFAS exposure through drinking water, as captured by ‘UCMR5’, which is affected by both observable socio-economic and urbanization factors as well as unmeasured spatial confounders. These factors may directly influence health outcomes, introducing potential confounding. Although our analysis focuses on waterborne PFAS, the diagram also marks other exposure routes—such as occupational sources, PFAS in air, and additional pollutants—that are unobserved and approximated through their assumed spatial structure. The diagram situates our target pathway within this broader causal context and underscores the role of both measured and unmeasured determinants in shaping associations between PFAS exposure and chronic disease outcomes.

Our final data tensor had dimensions (5,495, 4, 13), corresponding to $N = 5,495$ geographic units, $L = 4$ exposure combinations (binary indicators for PFOA and PFOS), and $O = 13$ outcomes. Spatial distance was defined using regional centroids, with adjacency constructed

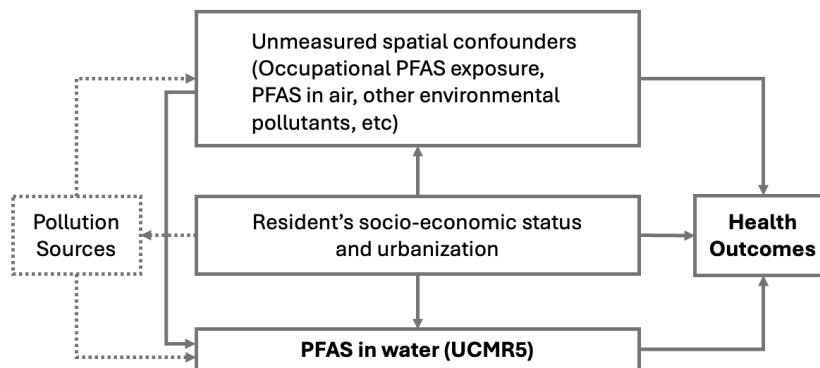


Figure 2: Conceptual diagram of PFAS health effect analysis.

via a $k = 4$ nearest-neighbors algorithm symmetrized by union of directed edges. The average number of neighbors per region is therefore slightly greater than 4. In **Supplement C.2** visualizes the PFAS distribution and disease distribution.

In both the propensity score model for chemical exposure and the outcome tensor model, we incorporate covariates related to industry employment (percentage of population employed in agriculture, construction, manufacturing, wholesale, retail, transportation, information, finance, professional, education, arts, other services, public administration) as well as a range of socio-economic indicators, including: median home value, the percentage of Hispanic/Latino residents, the percentage of foreign-born residents, median income, the percentage of individuals aged 19 to 64 with health insurance, and the percentage of residents holding a bachelor’s degree or higher. Population density is included as a proxy for urbanization. The Tucker ranks are tuned via 5-fold cross-validation over the grids $r_1 \in \{1, \dots, 10\}$, $r_2 \in \{1, \dots, 3\}$, and $r_3 \in \{1, \dots, 5\}$. To improve the robustness of missingness imputation in the tensor, we implement a 5-fold cross-fitting procedure.

5.2 Results

5.2.1 Competing Methods

We compare five estimation approaches, each combining an outcome model with a propensity score model under the augmented inverse probability weighting (AIPW) framework as described in Section 4.3. **Spatial-Tensor**: Our proposed method using spatial tensor completion for outcomes and eigenvector-adjusted multinomial logit for propensities. **Tensor**: Tensor completion without spatial adjustment for outcomes, with standard multinomial logit for propensities. **Spatial-PS**: Standard regression fit separately per outcome, with eigenvector-adjusted multinomial logit for propensities (Davis et al. 2019). **Standard Regression**: Separate regressions per outcome with standard multinomial logit for propensities. **Augmented Regression**: Separate regressions per outcome, with standard multinomial logit for propensities.

5.2.2 Full Factorial Exposure Effects

Figure 3 presents estimated odds ratios across the full factorial exposure structure, comparing our proposed spatial tensor method with four alternative approaches. Regression-based methods produced inflated and often implausible associations, with odds ratios exceeding 3.0 for several outcomes. In contrast, tensor-based methods provided more conservative and internally consistent estimates, with odds ratios typically below 1.05.

The stark differences between methods reflect distinct approaches to handling missing potential outcomes and confounding. Regression-based estimate each outcome independently, neither borrowing strength across the 13 disease endpoints nor imposing structure on the counterfactual outcome surface. Tensor-based approaches, by contrast, exploit low-rank structure to pool information across outcomes and exposures simultaneously, and regularize estimates through the assumption that a small number of latent factors explain most

outcome variation, leading to improved efficiency. The spatial tensor method further incorporates graph Laplacian eigenvectors to approximate unmeasured spatial confounders, removing spurious geographic associations while preserving efficiency (substantially narrower confidence intervals) gains from joint modeling.

The non-spatial tensor identified significant adverse associations for PFOS with four outcomes and one for PFOA, while combined PFOA+PFOS was associated with elevated odds for nearly all outcomes. Interestingly, PFOA appeared protective for asthma, whereas PFOS had the opposite effect. After adjusting for unmeasured spatial confounders via 10 selected eigenvectors, the spatial tensor attenuated most associations: only two adverse health effects for PFOS (tooth loss, obesity) and one protective effect for PFOA+PFOS remained significant (COPD).

Sensitivity analyses in **Supplement C.2** demonstrate that including additional eigenvectors progressively attenuates effect estimates, indicating that unadjusted models conflate geographic confounding with causal effects. Cross-validation confirms the spatial tensor achieves superior out-of-sample prediction, validating improvements in both confounding control and predictive accuracy.

5.2.3 Marginal Exposure Effects

To summarize exposure effects across the factorial structure, we define marginal effects that average over the distribution of the other exposure—quantifying the expected impact of each PFAS chemical regardless of whether the other is present or absent, and relevant for regulatory policy. Figure 4 displays the resulting marginal odds ratios with 95% confidence intervals, comparing the spatial-tensor and non-spatial tensor models. Detailed calculations are provided in **Supplement C.2**. After adjusting for unmeasured spatial confounders via the spatial-tensor approach, PFOA showed no significant associations with any outcome

except for a modest protective effect on asthma (OR = 0.995, 95% CI: 0.991-0.999). In contrast, PFOS retained significant adverse associations with hypertension (OR = 1.026, 95% CI: 1.001-1.052), tooth loss (OR = 1.019, 95% CI: 1.005-1.033), asthma (OR = 1.007, 95% CI: 1.003-1.012), and obesity (OR = 1.023, 95% CI: 1.001-1.046).

5.2.4 Latent Factor Structure

Figure 5 (top panel) visualizes the latent geographic structure captured by the spatial tensor model through the factor matrix \mathbf{U}_1 . We applied K-means clustering to the factor loadings to identify eight (the selected rank of \mathbf{U}_1) distinct spatial patterns. The dominant pattern (dark green) is concentrated throughout much of the Eastern United States, and the second cluster (orange) appears concentrated in parts of the South-Central region, while smaller clusters capture localized geographic features such as the Pacific Coast, Upper Midwest.

Figure 5 (bottom panel) displays the latent disease structure encoded in factor matrix \mathbf{U}_3 , which captures shared patterns of outcome variation across the 13 chronic diseases. Component 1 (red) reflects a dominant shared morbidity factor, with nearly all diseases loading positively, representing common risk pathways that affects multiple chronic conditions simultaneously. Components 2 and 3 capture more nuanced contrasts across disease groups. Interpreting these finer structural patterns in terms of specific biological mechanisms remains an important direction for future research, as they may reveal how chemical exposures align with distinct pathways of chronic disease etiology. These factors demonstrate the tensor model’s ability to capture and exploit outcome structure when estimating exposure effects.

6 Discussion

To estimate the effects of PFAS chemicals on a range of health outcomes, we propose a spatial causal tensor completion framework for multiple binary exposures and outcomes,

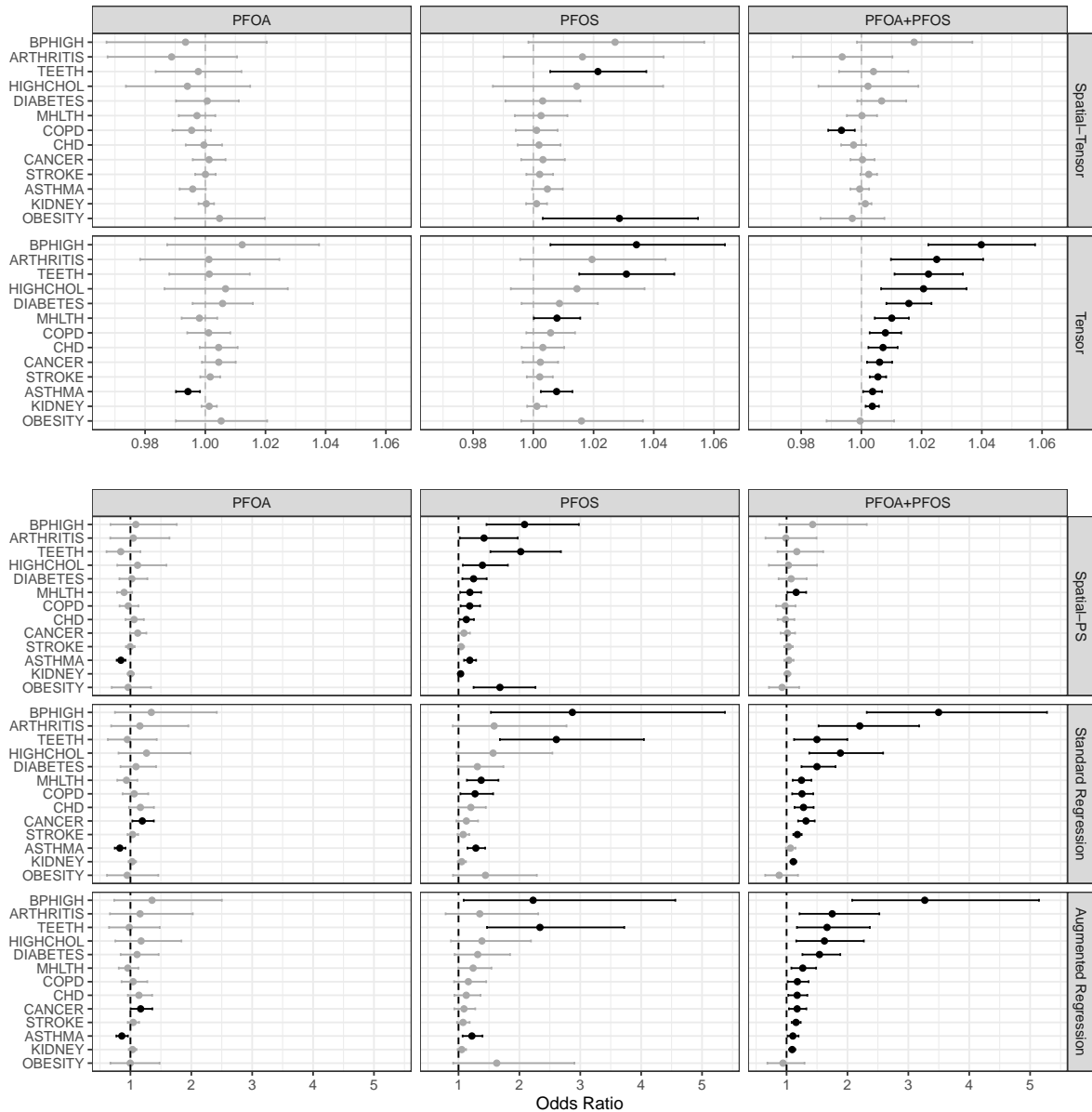


Figure 3: Estimated odds ratios for 13 disease outcomes under PFOA, PFOS, and combined exposures across different models. Black indicates statistically significant associations; gray indicates non-significant results. Note that the x-axis scales differ across panels, so effect sizes are not directly comparable between the top and bottom rows.

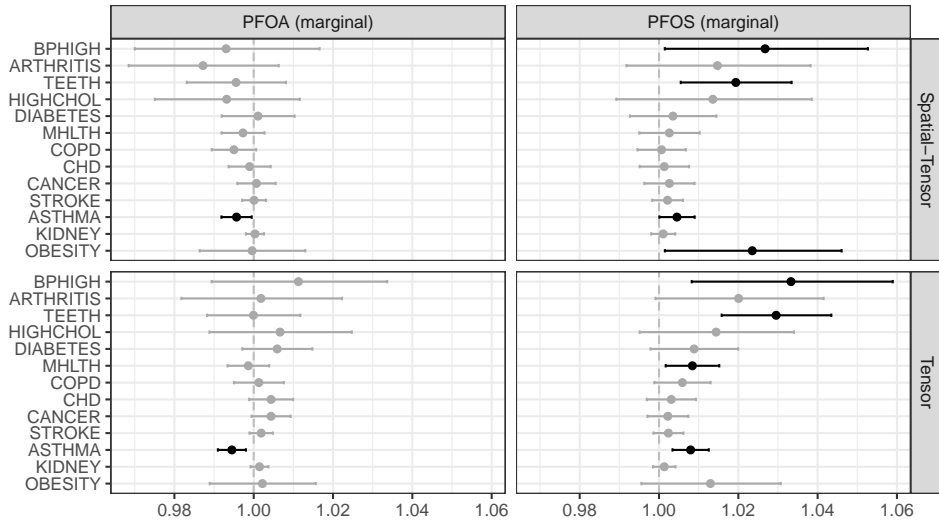


Figure 4: Estimated marginal odds ratios for 13 disease outcomes under PFOA and PFOS exposures across different models. Black indicates statistically significant associations; gray indicates non-significant results.

integrating a low-rank tensor structure to pool information and spectral adjustment to approximate unmeasured spatial confounders, embedded within a projected-gradient descent algorithm. This design enables causal inference in the presence of spatial confounding and pervasive missingness. Theoretically, we establish the Frobenius-error bounds for the completed outcome tensor, showing estimation error depends on spatial approximation error, propensity-score estimation error, tensor rank, and others. Extensive simulations corroborate these findings, showing our estimator achieves efficiency gains against competing approaches.

Applied to national PFAS monitoring data linking PFOA/PFOS exposures with 13 chronic disease outcomes, our method yields substantially more conservative odds ratio estimates compared to existing alternatives. The substantial attenuation following spatial adjustment demonstrates the importance of accounting for latent geographic confounding. The alternatives identified multiple significant adverse associations (bottom panel of Figure 3). After incorporating tensor structure and latent spatial confounding, our model (top panel) yielded a far sparser set of significant and attenuated effects. This systematic shift from

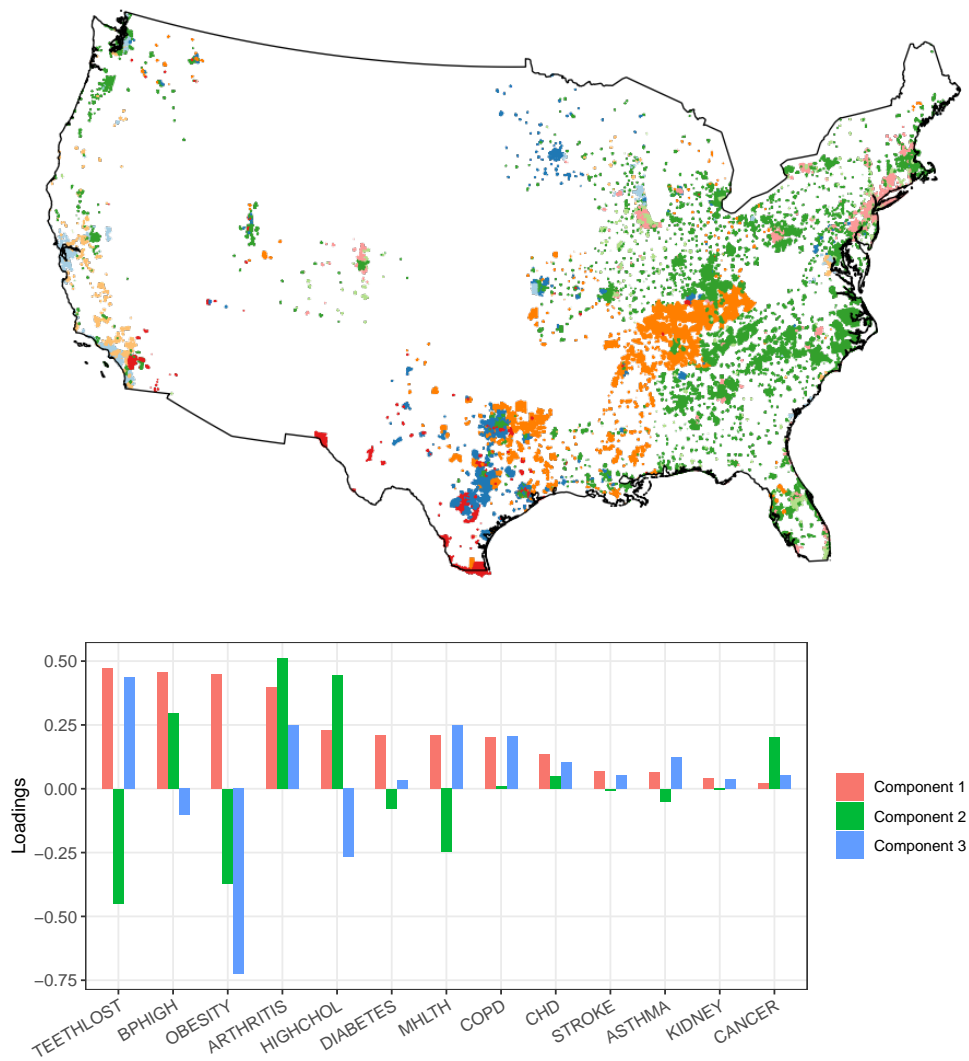


Figure 5: Latent factors in the spatial tensor model. Top: Clustering of geographic units based on the location factor $\widehat{\mathbf{U}}_1$. Bottom: Loadings in outcome factor $\widehat{\mathbf{U}}_3$.

near-universal associations to selective findings suggests that conventional approaches may substantially inflate effect estimates when spatially-structured confounders remain uncontrolled.

Our findings have implications for interpreting the broader PFAS epidemiologic literature. Recent meta-analyses have demonstrated fairly consistent adverse associations between PFOA/PFOS exposure and hypertension ([Xiao et al. 2023](#)), blood lipid levels ([Liu et al. 2023](#)), and particular types of cancer ([Bartell & Vieira 2021](#)). Our spatially-adjusted results for PFOS and hypertension are consistent with this meta-analytic evidence. However, for many other health outcomes, the epidemiologic evidence remains inconsistent, as exemplified by studies of diabetes ([Gui et al. 2023](#), [Sun et al. 2018](#)) and obesity ([Frangione et al. 2024](#)). Our results suggest that inadequate control for geographic confounding may have inflated effect estimates. The heterogeneity across studies may thus reflect not only differences in exposure levels, population characteristics, but also different spatial confounding bias.

Our analysis is subject to several limitations. First, disease outcomes are derived from model-based prevalence estimates rather than clinical measurements ([CDC 2023](#)), introducing measurement error that likely attenuates observed associations. Second, exposure assessment relies on public water system monitoring and does not capture individual-level exposure variation or non-water exposure routes. Third, the cross-sectional linkage of 2023-2024 water monitoring data with 2017-2018 health outcomes limits causal inference, though the long environmental persistence and biological half-lives of PFAS partially mitigate temporal misalignment. Fourth, while our method adjusts for smooth spatial confounding through Laplacian eigenvectors, it cannot address all forms of unmeasured confounding, particularly individual-level factors uncorrelated with geography. Finally, our factorial design treats exposure as binary indicators rather than modeling dose-response relationships at varying concentration levels.

Several promising directions exist for extending this framework. First, incorporating continuous exposures through functional tensor representations would enable modeling of dose-response relationships rather than binary exposure indicators. Second, while the tensor framework naturally produces unit-level treatment effect estimates, developing valid inference procedures for heterogeneous and individualized causal effects remains an important methodological challenge. Third, extending the approach to longitudinal settings with time-varying exposures and outcomes would accommodate dynamic exposure patterns and enhance its applicability in environmental health and related domains.

SUPPLEMENTARY MATERIAL

Supplement A: Full Theorem, proof and interpretation. **Supplement B:** Detailed algorithm. **Supplement C:** Additional results with PFAS data analysis. **Supplement D:** Simulation study.

References

- Abadie, A., Agarwal, A., Dwivedi, R. & Shah, A. (2024), ‘Doubly Robust Inference in Causal Latent Factor Models’, *arXiv preprint arXiv:2402.11652* .
- Agarwal, A., Shah, D. & Shen, D. (2020), ‘Synthetic interventions’, *arXiv preprint arXiv:2006.07691* .
- Auerbach, J., Slawski, M. & Zhang, S. (2022), ‘Tensor completion for causal inference with multivariate longitudinal data: A reevaluation of covid-19 mandates’, *arXiv preprint arXiv:2203.04689* .
- Bang, H. & Robins, J. M. (2005), ‘Doubly robust estimation in missing data and causal inference models’, *Biometrics* **61**(4), 962–973.

- Barry, V., Winqvist, A. & Steenland, K. (2013), ‘Perfluorooctanoic acid (pfoa) exposures and incident cancers among adults living near a chemical plant’, *Environmental health perspectives* **121**(11-12), 1313–1318.
- Bartell, S. M. & Vieira, V. M. (2021), ‘Critical review on pfoa, kidney cancer, and testicular cancer’, *Journal of the Air & Waste Management Association* **71**(6), 663–679.
- Biggeri, A., Stoppa, G., Facciolo, L., Fin, G., Mancini, S., Manno, V., Minelli, G., Zamagni, F., Zamboni, M., Catelan, D. et al. (2024), ‘All-cause, cardiovascular disease and cancer mortality in the population of a large italian area contaminated by perfluoroalkyl and polyfluoroalkyl substances (1980–2018)’, *Environmental Health* **23**(1), 42.
- Bobb, J. F., Valeri, L., Claus Henn, B., Christiani, D. C., Wright, R. O., Mazumdar, M., Godleski, J. J. & Coull, B. A. (2015), ‘Bayesian kernel machine regression for estimating the health effects of multi-pollutant mixtures’, *Biostatistics* **16**(3), 493–508.
- Candes, E. J. & Plan, Y. (2010), ‘Matrix completion with noise’, *Proceedings of the IEEE* **98**(6), 925–936.
- Candes, E. & Recht, B. (2009), ‘Exact matrix completion via convex optimization’, *Communications of the ACM* **55**(6), 111–119.
- Carrico, C., Gennings, C., Wheeler, D. C. & Factor-Litvak, P. (2015), ‘Characterization of weighted quantile sum regression for highly correlated data in a risk analysis setting’, *Journal of agricultural, biological, and environmental statistics* **20**, 100–120.
- CDC (2023), ‘Places: Local data for better health, census tract data 2023 release’.
- Chernozhukov, V., Chetverikov, D., Demirer, M., Duflo, E., Hansen, C., Newey, W. & Robins, J. (2018), ‘Double/debiased machine learning for treatment and structural parameters’.
- Davis, M. L., Neelon, B., Nietert, P. J., Hunt, K. J., Burgette, L. F., Lawson, A. B. &

- Egede, L. E. (2019), ‘Addressing geographic confounding through spatial propensity scores: A study of racial disparities in diabetes’, *Statistical Methods in Medical Research* **28**(3), 734–748.
- Dupont, E., Wood, S. N. & Augustin, N. H. (2022), ‘Spatial+: A novel approach to spatial confounding’, *Biometrics* **78**(4), 1279–1290.
- Fenton, S. E., Ducatman, A., Boobis, A., DeWitt, J. C., Lau, C., Ng, C., Smith, J. S. & Roberts, S. M. (2021), ‘Per- and polyfluoroalkyl substance toxicity and human health review: Current state of knowledge and strategies for informing future research’, *Environmental toxicology and chemistry* **40**(3), 606–630.
- Frangione, B., Birk, S., Benzouak, T., Rodriguez-Villamizar, L. A., Karim, F., Dugandzic, R. & Villeneuve, P. J. (2024), ‘Exposure to perfluoroalkyl and polyfluoroalkyl substances and pediatric obesity: a systematic review and meta-analysis’, *International Journal of Obesity* **48**(2), 131–146.
- Gaines, L. G. (2023), ‘Historical and current usage of per- and polyfluoroalkyl substances (pfas): A literature review’, *American Journal of Industrial Medicine* **66**(5), 353–378.
- Gao, C., Chen, H., Zhang, A. R. & Yang, S. (2025), ‘Causal inference on sequential treatments via tensor completion’, *arXiv preprint arXiv:2511.15866* .
- Gao, C., Yang, S. & Kim, J. K. (2023), ‘Soft calibration for selection bias problems under mixed-effects models’, *Biometrika* **110**(4), 897–911.
- Gao, C., Zhang, Z. & Yang, S. (2024), ‘Causal customer churn analysis with low-rank tensor block hazard model’, *arXiv preprint arXiv:2405.11377* .
- Gilbert, B., Datta, A., Casey, J. A. & Ogburn, E. L. (2021), ‘A causal inference framework for spatial confounding’, *arXiv preprint arXiv:2112.14946* .

- Guan, Y., Page, G. L., Reich, B. J., Ventrucci, M. & Yang, S. (2023), ‘Spectral adjustment for spatial confounding’, *Biometrika* **110**(3), 699–719.
- Gui, S.-Y., Qiao, J.-C., Xu, K.-X., Li, Z.-L., Chen, Y.-N., Wu, K.-J., Jiang, Z.-X. & Hu, C.-Y. (2023), ‘Association between per- and polyfluoroalkyl substances exposure and risk of diabetes: A systematic review and meta-analysis’, *Journal of Exposure Science & Environmental Epidemiology* **33**(1), 40–55.
- Joubert, B. R., Kioumourtzoglou, M.-A., Chamberlain, T., Chen, H. Y., Gennings, C., Turyk, M. E., Miranda, M. L., Webster, T. F., Ensor, K. B., Dunson, D. B. et al. (2022), ‘Powering research through innovative methods for mixtures in epidemiology (prime) program: Novel and expanded statistical methods’, *International Journal of Environmental Research and Public Health* **19**(3), 1378.
- Kang, S., Franks, A., Audirac, M., Braun, D. & Antonelli, J. (2023), ‘Partial identification and unmeasured confounding with multiple treatments and multiple outcomes’, *arXiv preprint arXiv:2311.12252* .
- Keil, A. P., Buckley, J. P., O’Brien, K. M., Ferguson, K. K., Zhao, S. & White, A. J. (2020), ‘A quantile-based g-computation approach to addressing the effects of exposure mixtures’, *Environmental health perspectives* **128**(4), 047004.
- Keller, J. P. & Szpiro, A. A. (2020), ‘Selecting a scale for spatial confounding adjustment’, *Journal of the Royal Statistical Society Series A: Statistics in Society* **183**(3), 1121–1143.
- Kolda, T. G. & Bader, B. W. (2009), ‘Tensor decompositions and applications’, *SIAM review* **51**(3), 455–500.
- Liu, B., Zhu, L., Wang, M. & Sun, Q. (2023), ‘Associations between per- and polyfluoroalkyl substances exposures and blood lipid levels among adults—a meta-analysis’, *Environmental health perspectives* **131**(5), 056001.

- Mao, X., Wang, H., Wang, Z. & Yang, S. (2024), ‘Mixed matrix completion in complex survey sampling under heterogeneous missingness’, *Journal of Computational and Graphical Statistics* **33**(4), 1320–1328.
- Marques, I., Kneib, T. & Klein, N. (2022), ‘Mitigating spatial confounding by explicitly correlating gaussian random fields’, *Environmetrics* **33**(5), e2727.
- NASEM et al. (2022), *Guidance on PFAS exposure, testing, and clinical follow-up*.
- Osama, M., Zachariah, D. & Schön, T. B. (2019), Inferring heterogeneous causal effects in presence of spatial confounding, *in* ‘International Conference on Machine Learning’, PMLR, pp. 4942–4950.
- Papadogeorgou, G., Choirat, C. & Zigler, C. M. (2019), ‘Adjusting for unmeasured spatial confounding with distance adjusted propensity score matching’, *Biostatistics* **20**(2), 256–272.
- Poulos, J., Albanese, A., Mercatanti, A. & Li, F. (2021), ‘Retrospective causal inference via matrix completion, with an evaluation of the effect of european integration on cross-border employment’, *arXiv preprint arXiv:2106.00788* .
- Prim, S.-N., Guan, Y., Yang, S., Rappold, A. G., Hill, K. L., Tsai, W.-L., Keeler, C. & Reich, B. J. (2025), ‘A spectral confounder adjustment for spatial regression with multiple exposures and outcomes’, *arXiv preprint arXiv:2506.09325* .
- Reich, B. J., Yang, S., Guan, Y., Giffin, A. B., Miller, M. J. & Rappold, A. (2021), ‘A review of spatial causal inference methods for environmental and epidemiological applications’, *International Statistical Review* **89**(3), 605–634.
- Rubin, D. B. (1974), ‘Estimating causal effects of treatments in randomized and nonrandomized studies.’, *Journal of educational Psychology* **66**(5), 688.

- Schnell, P. M. & Papadogeorgou, G. (2020), ‘Mitigating unobserved spatial confounding when estimating the effect of supermarket access on cardiovascular disease deaths’, *arXiv preprint arXiv:1907.12150* .
- Sun, Q., Zong, G., Valvi, D., Nielsen, F., Coull, B. & Grandjean, P. (2018), ‘Plasma concentrations of perfluoroalkyl substances and risk of type 2 diabetes: A prospective investigation among us women’, *Environmental health perspectives* **126**(3), 037001.
- Thaden, H. & Kneib, T. (2018), ‘Structural equation models for dealing with spatial confounding’, *The American Statistician* **72**(3), 239–252.
- US EPA (2024), ‘Epa’s pfa analytics tool’. Accessed: 2024-08-12.
URL: <https://echo.epa.gov/trends/pfas-tools>
- Walker, K., Herman, M., Eberwein, K. & Walker, M. K. (2021), ‘Package “tidycensus”, *MIT* .
- Wiecha, N., Hoppin, J. A. & Reich, B. J. (2025), ‘Two-stage estimators for spatial confounding with point-referenced data’, *Biometrics* **81**(3), ujaf093.
- Wu, J. & Franks, A. (2025), ‘A latent factor panel approach to spatiotemporal causal inference’, *arXiv preprint arXiv:2509.10974* .
- Xiao, F., An, Z., Lv, J., Sun, X., Sun, H., Liu, Y., Liu, X. & Guo, H. (2023), ‘Association between per- and polyfluoroalkyl substances and risk of hypertension: A systematic review and meta-analysis’, *Frontiers in public health* **11**, 1173101.
- Yang, S. (2018), ‘Propensity score weighting for causal inference with clustered data’, *Journal of Causal Inference* **6**(2), 20170027.
- Zhen, Y. & Wang, J. (2024), ‘Nonnegative tensor completion for dynamic counterfactual prediction on covid-19 pandemic’, *The Annals of Applied Statistics* **18**(1), 224–245.